

Charged particle scattering in dipolarized magnetotail

A. S. Lukin^{1,2}, A. V. Artemyev^{1,3}, A. A. Petrukovich¹, and X.-J. Zhang³

¹Space Research Institute of the Russian Academy of Sciences (IKI), 84/32 Profsoyuznaya Str, Moscow, Russia, 117997; as.lukin.phys@gmail.com

²Faculty of Physics, National Research University Higher School of Economics, 21/4 Staraya Basmannaya Ulitsa, Moscow, Russia, 105066

³Department of Earth, Planetary, and Space Sciences, University of California, 595 Charles E Young Dr E, Los Angeles, CA, California, USA, 90095; aartemyev@igpp.ucla.edu

May 13, 2021

Abstract

The Earth's magnetotail is characterized by stretched magnetic field lines. Energetic particles are effectively scattered due to the field-line curvature, which then leads to isotropization of energetic particle distributions and particle precipitation to the Earth's atmosphere. Measurements of these precipitation at low-altitude spacecraft are thus often used to remotely probe the magnetotail current sheet configuration. This configuration may include spatially localized maxima of the curvature radius at equator (due to localized humps of the equatorial magnetic field magnitude) that reduce the energetic particle scattering and precipitation. Therefore, the measured precipitation patterns are related to the spatial distribution of the equatorial curvature radius that is determined by the magnetotail current sheet configuration. In this study, we show that, contrary to previous thoughts, the magnetic field line configuration with the localized curvature radius maximum can actually enhance the scattering and subsequent precipitation. The spatially localized magnetic field dipolarization (magnetic field humps) can significantly curve magnetic field lines far from the equator and create off-equatorial minima in the curvature radius. Scattering of energetic particles in these off-equatorial regions alters the scattering (and precipitation) patterns, which has not been studied yet. We discuss our results in the context of remote-sensing the magnetotail current sheet configuration with low-altitude spacecraft measurements.

Introduction

Configuration of the Earth's magnetotail current sheet determines its stability and controls many energetic events, e.g., magnetospheric substorms^{1,2,3} and plasma convection^{4,5}. In-situ spacecraft measurements of the magnetotail plasma and magnetic field are rather limited, as spacecraft (even multiple) can only simultaneously probe few spatially localized regions (see Refs.^{6,7,8,9,10} for examples of probing of the magnetotail current sheet configuration with in-situ multi-spacecraft missions). Thus, alternative methods to examine the current sheet configuration can be especially useful. Statistical methods¹¹ have then been used to reconstruct the current sheet configuration by fitting to

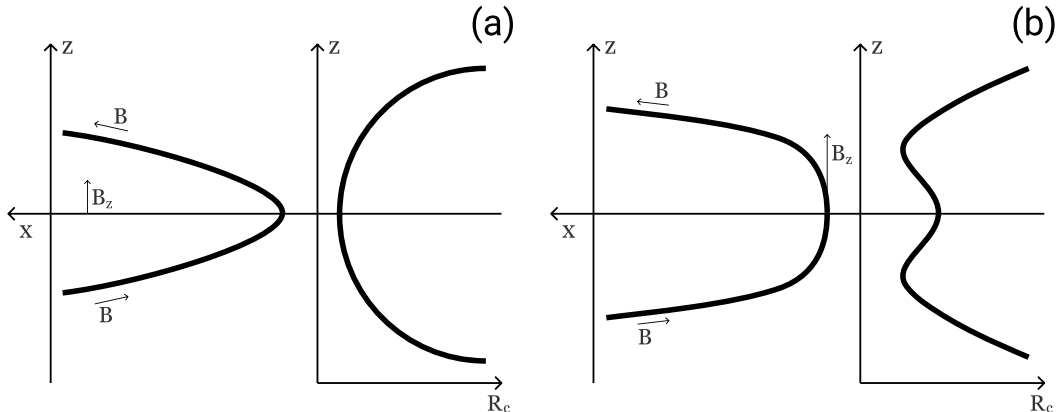


Figure 1: Schematic view of magnetic field lines and field line curvature radius in the magnetotail current sheet for two typical configurations: (a) quite-time thin current sheet, (b) current sheet with the embedded dipolarization front.

the model^{12,13,14} or via data mining approaches^{15,16,17}. This set of methods provides quite accurate description of the magnetotail current sheet, but very restricted to the time-scale of evolution of the current sheet configuration, i.e. the statistical reconstruction shows some averaged (typical) configuration that may slowly evolve with the time-scale of the evolution of input model parameters (that are often geomagnetic indexes, see Refs.^{11,18}). The second group of methods considers low altitude spacecraft measurements of charged particle precipitations from the magnetotail for reconstruction of instantaneous current sheet configuration^{19,20,21}. These methods are essentially based on the theory of charged particle scattering in the curved magnetic field lines of the magnetotail current sheet^{22,23,24,25,26}, and our study develops this theory for a complex current sheet configurations.

Schematic in Fig. 1(a) shows that magnetic field lines in a quite-time thin current sheet are well stretched due to smallness of the ratio of magnetic field components, $B_z/B_{0x} \ll 1$ (see for details Refs.^{6,9}). Magnetized electrons and ions are scattered in such magnetic field configuration, i.e. there is a jump of magnetic moment $\mu = mv_{\perp}^2/B$ ($B = |\mathbf{B}|$ and v_{\perp} is the transverse component of particle velocity) when particles cross the region with the smallest R_c/ρ (R_c is magnetic field line curvature radius, ρ is the particle gyroradius). For the most typical $R_c/\rho > 1$ magnetotail configuration^{6,27} such jumps of a magnetic moment can be considered within the theory of the adiabatic invariant destruction in the slow-fast nonlinear systems^{28,29,30}. The basic model of this destruction has been constructed for magnetic traps in laboratory plasma^{31,32,33,34} and then generalized to the current sheets in the planetary magnetotails^{35,25}. Comprehensive numerical investigations result in the empirical models of $\Delta\mu$ jump as a function of R_c/ρ . For a fixed particle energy these models provide $\Delta\mu$ as a function of magnetic field configuration^{36,37,38,39}. The main model prediction is threshold of B_z/B_{0x} for strong scattering (significant $\Delta\mu$). Such threshold provides the basement for analysis of low-altitude observations for remote probing the magnetotail current sheet configuration^{40,41,42}. These models, however, have been developed for the *classical* current sheet with a single R_c minimum at the equatorial ($B_x = 0$) plane (see Fig. 1(a)).

If there is only equatorial R_c minimum, any suppression of equatorial scattering (decrease of precipitating fluxes on the low-altitude spacecraft) should be interpreted as a local increase of B_z/B_0 ratio^{43,44}. This interpretation may be invalid for more complex current sheet configurations with

off-equatorial R_c minima^{45,46}. One of such configurations is shown in Fig. 1(b) where so-called dipolarized current sheet is presented. The transient magnetic reconnection in the middle (far from the Earth) magnetotail generates very large amplitude perturbations of B_z (dipolarization fronts, see Refs. ^{47,48,49,50}). These perturbations propagate earthward and breaking in the near-Earth current sheet^{51,52}. Thus, in the near-Earth current sheet we can observe a magnetic field configuration with a sharp B_z gradient ($\partial B_z/\partial x$) and strong B_z enhancement. Such an enhancement should decrease the equatorial R_c and suppress charged particle scattering, but large $\partial B_z/\partial x$ may create additional off-equatorial R_c minima and enhance the scattering. Therefore, for accurate interpretation of precipitating particle fluxes on low-altitude spacecraft there is a need for parametric investigation of the charged particle scattering in the magnetotail current sheet configuration with the embedded dipolarization front.

In this study we investigate charged particle scattering in such magnetotail current sheet configuration. First, we introduce the magnetic field model in Sect. 1. Then the massive test particle simulations are used to show how the current sheet and dipolarization front parameters affect the efficiency of charged particle scattering. Main results of these simulations are shown in Sect. 2. We also modify the analytical model of charged particle scattering in the current sheet³⁵ to explain effects of off-equatorial R_c minima (see Sect. 3). Then we discuss obtained results and list main conclusions in Sect. 4.

1 Charged particle dynamics

The magnetic field configuration of the magnetotail current sheet around the equatorial plane (where main particle scattering occurs) can be fitted by a simple 1D model with $B_z = \text{const}$ and $B_x = B_{0x} \cdot (z/L_z)$, where L_z is the current sheet thickness. The curvature radius for this model has a minimum $\min R_c = L_z B_z / B_{0x}$ at the equator $z = 0$, where the charged particle gyroradius maximizes $\rho = \sqrt{2Emc^2}/eB_z$ where E , m , e are particle energy, mass, and charge. To describe the dipolarization front embedded into the current sheet, we modify B_z field as:

$$B_z = B_{+z} + 0.5(B_{-z} - B_{+z})(1 - \tanh(x/L_x)) \quad (1)$$

where L_x is the front thickness, and we locate the dipolarization front at $x = 0$. Far from the dipolarization front $B_z = B_{-z}$ for $x < 0$ and $B_z = B_{+z}$ for $x > 0$ where $B_{-z} > B_{+z}$. Three main system parameters are B_{+z}/B_{0x} , B_{-z}/B_{0x} , and L_x/L_z . Let us discuss ranges of these parameters derived from spacecraft observations in the near-Earth magnetotail. The current sheet thickness L_z varies from 500 km to 5000 km for most of observed magnetotail current sheets^{9,27}, and L_z is larger for post-dipolarization current sheet⁵³. The dipolarization front thickness L_x is generally smaller than 1000 km (see Refs. ^{54,55}) and can be as small as 300 – 500 km (see e.g., Ref. ^{56,57}). The magnetic field magnitude of the dipolarization front is comparable to the current sheet magnetic field, $B_{-z} \sim B_{0x}$, and is larger than the background $B_{+z} \sim B_{-z} \times [0.1, 0.5]$ (see statistics in Refs. ^{58,59}).

Figure 2(a) shows magnetic field line configuration for typical parameters of the current sheet and dipolarization front. Ahead the front ($x_0 > 0$) there are stretched magnetic field lines (parabolic shape $x \sim z^2$) with a curvature radius minimum, $R_c = L_z B_z / B_{0x}$, at the equatorial plane, where energetic particles are expected to be scattered. At the front the magnetic field line configuration changes and the curvature radius at the equator increases significantly. For some field lines there is almost no curvature at the equator, $R_c \rightarrow \infty$. However, due to the strong $dB_z/dx \sim 1/L_x$ gradient, there are two new off-equatorial R_c minima. Behind the dipolarization front ($x_0 < 0$) the current sheet configuration includes parabolic magnetic field lines around the equator (but the curvature radius there $R_c = L_z B_{-z} / B_{0x}$ is much larger than this radius ahead the front). These lines cross the

front dB_z/dx gradient, where a local minimum of the curvature radius may occur. Thus, energetic particle scattering in such magnetic field configuration strongly depends on the particle pitch-angle (i.e., location of particle mirror points where $E = \mu B$), because particles with smaller pitch-angles can reach off-equatorial minima of the curvature radius.

The scattering efficiency is determined by $\kappa = \min \sqrt{R_c/\rho}$ parameter⁶⁰, and thus depends on the magnetic field magnitude profile $B(s)$ along field lines: $s = \int_0^z B(x, z) dz / B_z(x)$ where $dx/dz = B_x(z)/B_z(x)$ is the magnetic field line equation. Contrast to the classical current sheet configuration with $B_z = \text{const}$, in the configuration from Fig. 2 the profile $B(s)$ varies with the x_0 , the field-line root position at the equator. Figure 2(b) shows several $B(s)$ profiles ahead the front, at the front, and behind the front (color coding are the same as in panel (a)). There are clear off-equatorial B minima for x_0 around the front.

2 Numerical results

To investigate charged particle scattering in the current sheet with the embedded dipolarization front we numerically integrate multiple trajectories described by 2D equations of motion: $\dot{\mathbf{r}} = \mathbf{v}$, $\dot{\mathbf{v}} = -e[\mathbf{v} \times \mathbf{B}]/m_e c$, where we use electron mass and charge (note the obtained results are applicable to ion scattering as well with the proper renormalization of energy to keep the same κ).

For 50 values of $x_0 \in [-5, 5]$ values and 12 equatorial pitch-angle values we numerically integrate $50 \times 12 \times 10^4 = 6 \times 10^6$ orbits. Each orbit starts at the mirror point $\mathbf{v} \cdot \mathbf{B} = 0$ above the equator (i.e. at $z > 0$) and ends on the opposite side of the equator at another mirror point. Initial $\mu_0 = mv_\perp^2/B = mv^2/B$ and final μ_f magnetic moments are calculated at mirror points, and this procedure reduces the magnetic moment fluctuations^{61,62}. These fluctuations are due to the fact that μ is the adiabatic (approximate) invariant and mv_\perp^2/B is the leading order approximation, whereas more accurate equations for μ can be derived using the improving procedure for adiabatic invariants⁶³.

Figure 3 shows boundaries μ_f/μ_0 of the distribution for different x_0 and $L_x/L_z = 10$ (very smoothed dipolarization front). We show μ_f/μ_0 for 5% of particles with largest μ_f/μ_0 and 5% of particles with the smallest μ_f/μ_0 (i.e., all μ_f/μ_0 are distributed somewhere between these two boundaries). This form of presentation allows us to compare numerical simulation results with analytical models of μ_f/μ_0 derived for the current sheet configuration (see Refs.^{37,64}; note these two models provide almost identical μ_f/μ_0 for equatorial pitch-angles below $\sim 60^\circ$ that are most interesting in the context of investigation of energetic particle scattering to the low altitudes). To make such a comparison we calculate $\kappa = \min \sqrt{R_c/\rho}$ for each x_0 and then evaluate the model μ_f/μ_0 for this κ . Note the model, derived in³⁷ has been constructed for the current sheet configuration with κ determined by the equatorial magnetic field line curvature, and thus model/simulations difference are due to off-equatorial scattering effects. Figure 3 shows that at large x_0 , where Eq. (1) gives $B_z = B_{+z}$, our numerical results are very close to the model, what verifies our scheme of μ_f/μ_0 calculations. Moreover, due to weak the dB_z/dx gradient for this simulation run ($L_x/L_z = 10$), even at x_0 around zero (the dipolarization front location, field-aligned particle scattering is well described by the model developed for the current sheet configuration. The model/simulations difference can be seen only for intermediate pitch-angles.

Figure 4 shows a scattering efficiency for moderately thin dipolarization front with $L_x/L_z = 1$. Small pitch-angle particles are scattered in agreement with predictions of the model constructed for the current sheet configuration, i.e. dB_z/dx is not sufficiently strong to change scattering. For intermediate pitch-angles the effect of dB_z/dx is seen better: there is a clear peak of scattering efficiency (maximum of μ_f/μ_0) around $x_0 \sim 0$ for $\alpha > 50^\circ$. Therefore, the dipolarization front

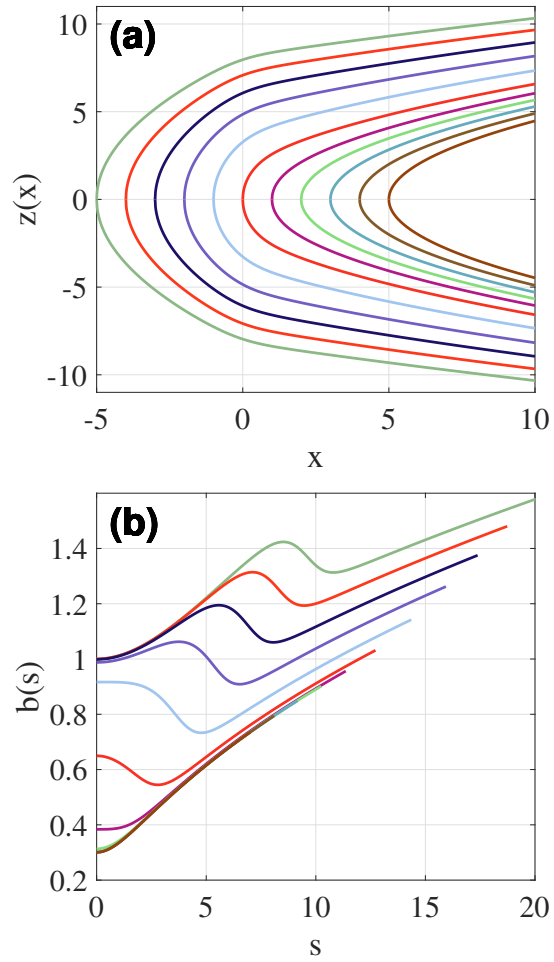


Figure 2: Magnetic field lines in the magnetotail current sheet with the embedded dipolarization front: $B_x = B_{0x} \cdot (z/L_z)$, B_z given by Eq. (1), $B_{-z}/B_{0x} = 1$, $B_{+z}/B_{0x} = 0.3$, $L_x/L_z = 0.15$.

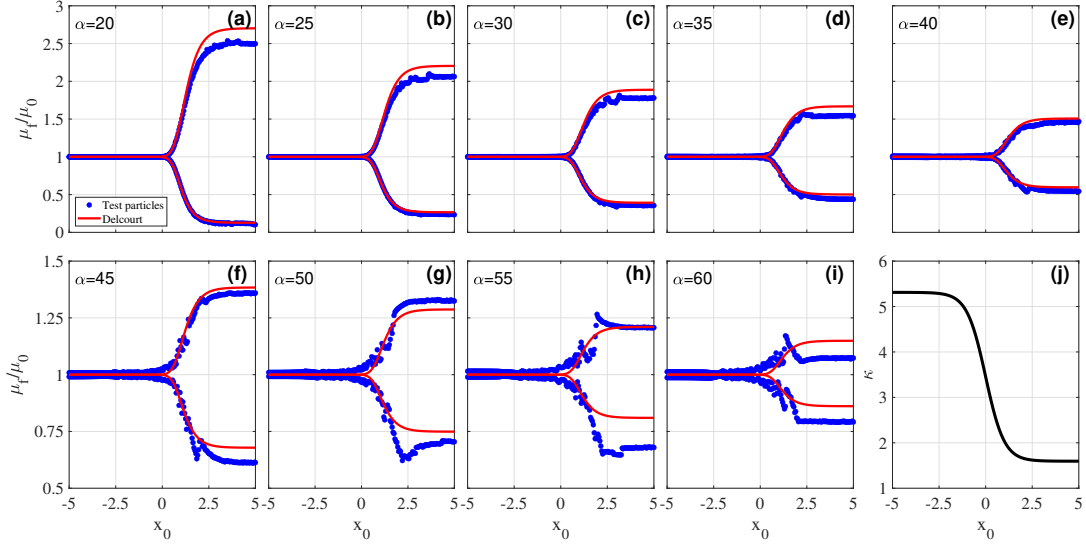


Figure 3: Comparison of μ_f/μ_0 for the analytical model of charged particle scattering in the current sheet³⁷(shown by red curves) and numerical results (shown by blue circles). Panels (a)-(i) correspond to different equatorial particle pitch angles (see the upper left corner of each panel). System parameters are: $L_x/L_z = 10$, $B_{-z}/B_{0x} = 1$, $B_{+z}/B_{0x} = 0.3$. Particle energy is chosen in such way to have $\kappa \sim 1.5$ for large $x_0 > 0$. Profile of $\kappa(x_0)$ evaluated at the equator is shown in the panel (j).

indeed can change the pattern of scattering and makes scattering spatially non-monotonic. But for $L_x/L_z = 1$ this effect is seen only for intermediate pitch-angles, far from the pitch-angle range corresponding to particle scattering to low-altitudes.

Figure 5 shows results for the thin dipolarization front with $L_x/L_z = 0.15$. So strong dB_z/dx moves the minimum κ position away from the equator (see Fig. 2(b)) and creates local (in x_0) maximum of the scattering efficiency (μ_f/μ_0 peaks) at $x_0 \sim 0$ for a wide pitch-angle range, including small pitch-angles. Such peaks of μ_f/μ_0 (or local minima of μ_f/μ_0) would be seen by low-altitude spacecraft as transient decreases/increases of precipitations along the spacecraft orbit⁴³. Note μ_f/μ_0 peaks/minima are not due to $\kappa(x_0)$ non-monotonical profile (see Fig. 5(f) showing equatorial $\kappa(x_0)$ and real $\kappa(x_0) = \min \sqrt{R_c(s)/\rho(s)}$ profiles), but due to change of the scattering pattern: instead of the single scattering at the equator, typical for the current sheet configuration, the strong dB_z/dx gradient creates two off-equatorial locations of scattering. Such scattering cannot be characterized by the single κ parameter and the scattering model should take into the account actual B profile along magnetic field lines.

Figure 6 compares patters of scattering $\Delta\mu_s/\mu_0 = \sqrt{\langle(\mu_f - \mu_0)^2\rangle}/\mu_0$, where $\langle\dots\rangle$ denotes the ensemble averaging, for three L_x/L_z values. The weak dB_z/dx gradient separates two regions with weak ($x_0 < 0$) and strong ($x_0 > 0$) scattering of all pitch-angles for $L_x/L_z = 10$ (see Fig. 6(a)). The stronger dB_z/dx gradient creates a local peak of scattering for intermediate pitch-angles around $x_0 \sim 0$, but does not affect weak scattering of small pitch-angle particles (see Fig. 6(a)). The strong dB_z/dx gradient creates the secondary maximum of scattering around $x_0 \sim 0$ for all pitch-angles.

Figure 7 shows the parametric investigation of the scattering efficiency. We fix $\alpha = 30^\circ$ and consider various $L_x/L_z \in [0.15, 0.5]$. The second peak of the scattering around the dipolarization

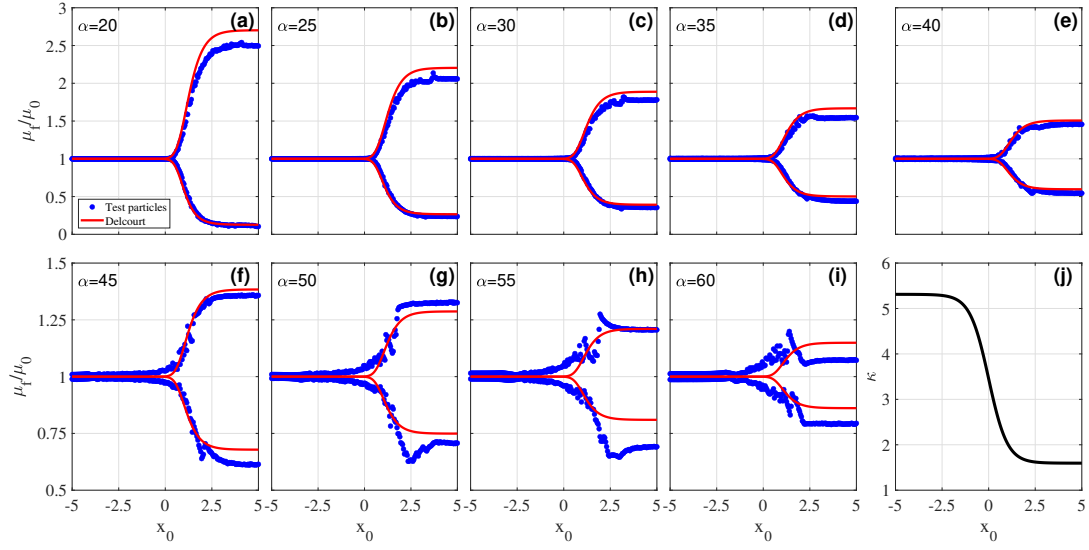


Figure 4: The same as in Fig. 3, but for $L_x/L_z = 1$.

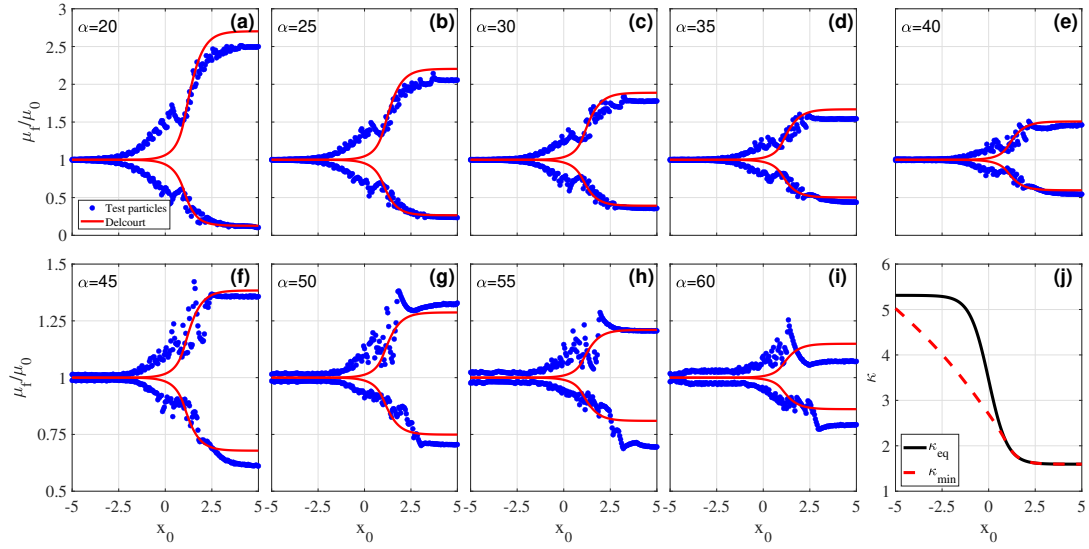


Figure 5: The same as in Fig. 3, but for $L_x/L_z = 0.15$. Red dashed line in panel (j) shows the minimal κ along field line, while solid black line shows equatorial κ .

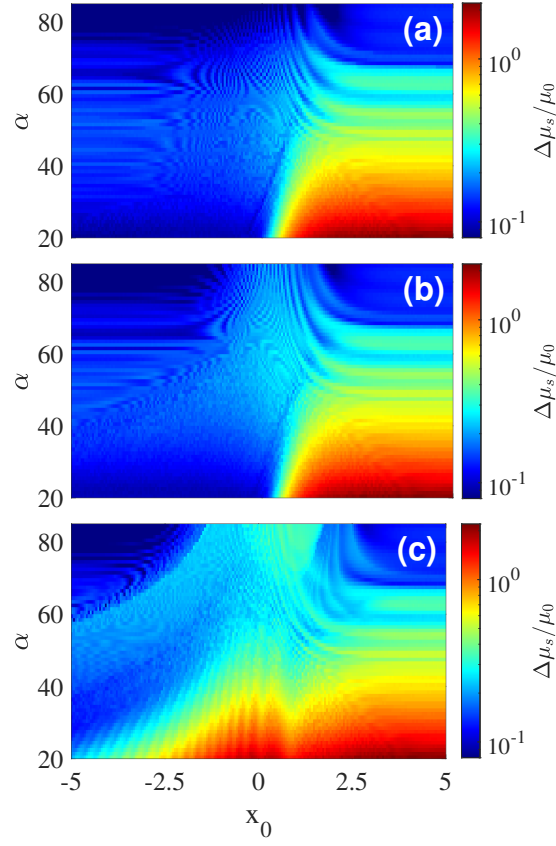


Figure 6: Distribution of $\Delta\mu_s/\mu_0$ in (x_0, α) space for system parameters $B_{-z}/B_{0x} = 1$, $B_{+z}/B_{0x} = 0.3$ and (a) $L_x/L_z = 10$, (b) $L_x/L_z = 1$, (c) $L_x/L_z = 0.15$.

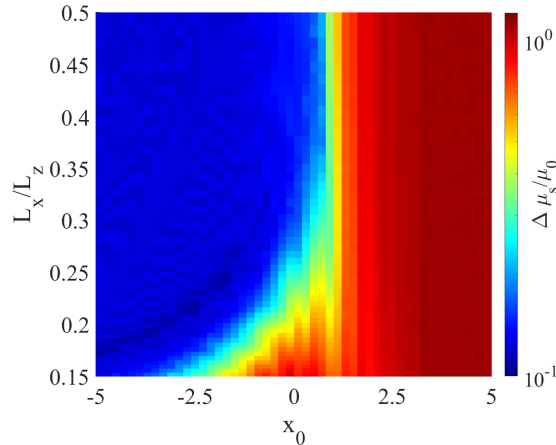


Figure 7: Distribution of $\Delta\mu/\mu_0$ in $(x_0, L_x/L_z)$ space for $\alpha = 30^\circ$.

front $x_0 \sim 0$ occurs for $L_x/L_z \sim 0.2 - 0.25$ for $B_{\pm z}/B_{0x} = 0.3, 1$ magnetic field magnitudes. Such L_x/L_z values are quite typical for the dipolarized magnetotail current sheet with $L_z \sim 3000$ km and $L_x \sim 300 - 1000$ km (see Refs. ^{54,65}). To confirm this double-peak scattering pattern we consider analytical theory of scattering in the next section.

3 Analytical estimates

The magnetic moment is the adiabatic invariant that should conserve with the exponential accuracy for the charged particle motion in a slowly time varying magnetic field (or a magnetic field slowly depending on coordinates) ^{66,67,68}. The general approach of evaluation of μ change has been proposed in Ref. ²⁹, but we are interested here only in the main part of this change, namely exponential term $\Delta\mu/\mu_0 \sim \exp(-f(\alpha)\kappa^2)$. For slow-fast dynamical systems (e.g., when gyrorotation is much faster than bounce motion) the general approach of estimate of this exponential term can be found in Refs. ^{30,69}. Such time separation of gyrorotation and bounce motion allows introduction of the magnetic field along the orbit as a function of a field-aligned coordinate, $B(s)$. Then, equation for function f takes the form ³⁵:

$$f(\mu^*) = \int_0^{\ell^*} \frac{b(\ell)d\ell}{\sqrt{1 - \mu^*b(\ell)}} \quad (2)$$

where $\mu^* = \sin^2 \alpha$ is the normalized magnetic moment independent on energy, α is the equatorial pitch-angle, $\ell = \Im(s)$ is the imaginary part of the dimensionless coordinate along magnetic field line, ℓ^* is a solution of $b(\Re(s) + i\ell) = 0$ equation, and $b(s) = B(s)/B_{0x}$ is dimensionless magnetic field magnitude. Being calculated, this exponential factor $\sim f(\mu^*)\kappa^2$ can explain the principal dependence of the scattering efficiency ($\Delta\mu/\mu_0$) on κ and equatorial pitch-angle. Note we restrict our consideration to this factor only and do not calculate the pre-exponential multiplication coefficient in $\Delta\mu/\mu_0$ expression. In Eq. (2) the integration is performed along the trajectory with $\mu^* = const$, but μ^* is only an approximate integral of motion that oscillates with an amplitude $\sim \kappa^{-2}$. Such a difference between actual and $\mu^* = const$ trajectories can affect the accuracy of $\Delta\mu$ evaluation ⁷⁰. This

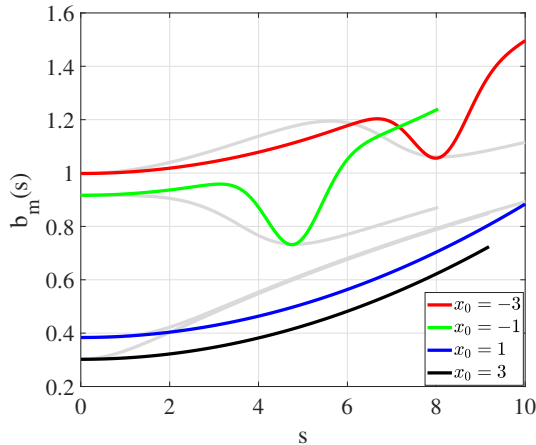


Figure 8: Model magnetic field profiles $b_m(s)$ that mimic results from Fig. 3.

effect does not change the exponential factor, but can change the pre-exponential multiplication coefficient^{71,30}. Therefore, test particle approaches are generally used to estimate this coefficient^{61,38}, and we do not derive it theoretically.

To describe $b(s)$ profiles from Fig. 2(b) in simpler form allowing calculation $b(\Re(s) + i\ell) = 0$ roots, we use the analytical model:

$$b_m = b_{eq} + as^2 - d \exp\left(-\frac{(s - s_{\min})^2}{\delta s^2}\right) \quad (3)$$

where $a = 5/1000$, $\delta s^2 = 0.75$, $b_{eq} = b_{eq}(x_0)$ is the normalized equatorial magnetic field, $d = b_{eq}(x_0) + c_2 s_{\min}^2 - b(s_{\min})$ for $s_{\min} > 0$, and s_{\min} is the coordinate of $b(\Re(s))$ minimum from Section 1.

Model (1) is much simpler than the full field model from Section 1 and provides almost analytical solutions for $b(\Re(s) + i\ell) = 0$. Moreover, this model is characterised by a finite $d^3b/ds^3|_{s=0}$ for all x_0 and do not have $d^3b/ds^3|_{s=0} \sim 0$ (see Fig. 8). Presence of a zero $d^3b/ds^3|_{s=0}$ (i.e. field line flattening at the equator) makes the standard scattering model³⁵ inapplicable, and requires derivation of more complicated equations instead Eq. (2), see, e.g., discussion in Ref.⁷².

Figure 8 shows that model (3) reproduces well the main features of the magnetic field $B(s)$ profiles for different x_0 . For large x_0 model shows the parabolic $B(s)$ with a single minimum at $s = 0$, and around $x_0 \sim 0$ model shows $B(s)$ profiles with off-equatorial minima.

Using model magnetic field (3) and $\kappa(x_0)$ from Fig. 5(j), we plot exponential factor $\kappa^2 f(\mu^*)$ in Fig. 9. Although this calculation does not take into account the pre-exponential multiplication factor, the main feature (two peak scattering, at $x_0 > 2$ and $x_0 \sim 0$) is well seen (compare Figs. 9 and 5). The second peak of scattering in the region of large b_{eq} (large B_z) is due to off-equatorial magnetic field minima (and corresponding curvature maxima). This effect can be found only in the current sheet with embedded dipolarization front having a sharp gradient dB_z/dx . Analytical estimates on Fig. 9 confirm the main numerical results of off-equatorial particle scattering at dipolarization front.

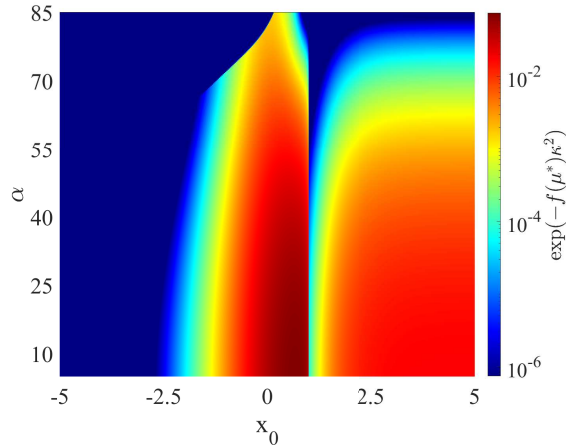


Figure 9: Distribution of the theoretical *scattering* factor in (α, x_0) space for $b_m(s)$ model from Fig. 8 and κ_{\min} profile shown in Fig. 5(j).

4 Discussion and Conclusions

There is the quite powerful approach of the magnetotail current sheet probing with precipitating energetic particle fluxes measured by low-altitude spacecraft^{19,20,21}. In this study we investigate patterns of scattering inducing such precipitations in the current sheet embedding dipolarization front. This magnetic field configuration contains two scattering regimes: the equatorial scattering in the pre-front current sheet (that has been discussed and described in details in Refs.^{35,36,73,64}) and off-equatorial scattering at the strong dB_z/dx gradient of the front. The second scattering regime is quite unusual, because it operates on the boundary of weak B_{-z} and strong B_{+z} fields. Within the classical models of the scattering in the current sheet, such B_z increase would be interpreted as a strong reduction of precipitation⁴³. We demonstrate, however, that due to strong dB_z/dx there are two off-equatorial regions of scattering instead of the single equatorial region. The off-equatorial R_c minima will enhance scattering and may form double-peak pattern of precipitations as seen on the low-altitude spacecraft^{43,44}. Therefore, the interpretation of measurements of such double-peak patterns might be reinvestigated with including direct equatorial measurements of the current sheet configuration.

There is a problem of a model construction for precipitation patters due to scattering in the current sheet with interchanging regions of dominant dB_x/dz and dB_z/dx gradients. If the model of scattering in the current sheet can be parametrized by a single parameter κ , any models of scattering in the current sheet with the dipolarization front should include at least two parameters to characterize contributions of dB_x/dz gradient (the equatorial κ) and dB_z/dx gradient (the off-equatorial R_c minimum). However, within such two parametrical model any interpretation of precipitation patterns derived from low-altitude spacecraft observations would be ambiguous, because enhancement/weakness of precipitation may be explained by two independent parameters, i.e. there are two scenarios describing any precipitation variations.

Therefore, probing of the current sheet configuration from precipitation measurements at low-altitude spacecraft should somehow distinguish between equatorial and off-equatorial scatterings. One of possible solutions is consideration of the time-scale of such scattering, i.e. energetic particle bounce period scale. The current sheet scattering is very stable and can operate for a sufficiently

long time to probe it with precipitations of plasma sheet ions (e.g., the most widespread type of analysis of low-altitude precipitations is based on processing of > 30 keV ion fluxes measured by Polar Operational Environmental Satellites^{20,21,41,42}). Scattering of such ions on dB_z/dx would mix spatial and temporal effects due to comparable time-scales of dipolarization front motion/evolution and bounce oscillations of ions. This problem, however, is not actual for energetic electrons that probe instantaneous magnetic field configuration much faster than it may evolve⁴⁰. In absence of accurate and energy/pitch-angle resolved electron measurements on existing low-altitude spacecraft such probing of the magnetotail configuration with electron measurements was not very widespread, but this approach should be more available with new low-altitude spacecraft missions^{74,75}

In conclusion, we have investigated scattering of energetic particles in the current sheet configuration with the embedded dipolarization front. Main findings of this study are:

- For a weak dB_z/dx gradient ($L_x/L_z \geq 1$) the magnetic field B_z increase suppresses scattering as expected for the quasi-1D current sheet model.
- For a strong dB_z/dx gradient ($L_x/L_z < 0.2$) the magnetic field lines at the front have off-equatorial curvature radius minima. Energetic particle scattering at these minima changes significantly the scattering pattern: there is no monotonic dependence of the scattering efficiency on B_z anymore.
- Off-equatorial scattering forms local peaks/minima of the scattering efficiency at the front. Such peaks/minima is seen for a wide pitch-angle range including field-aligned particles.

Acknowledgments

The work of A.S.L. was supported by the Russian Scientific Foundation, project 17-72-20134. X.-J.Z. acknowledges support from NASA grants 80NSSC20K1270.

Data Availability

This is theoretical study, and all figures are plotted using numerical solutions of equations provided with the paper. The data used for figures and findings in this study are available from the corresponding author upon reasonable request.

References

- [1] D. N. Baker, T. I. Pulkkinen, V. Angelopoulos, W. Baumjohann, and R. L. McPherron. Neutral line model of substorms: Past results and present view. *J. Geophys. Res.*, 101:12975–13010, June 1996. doi: 10.1029/95JA03753.
- [2] V. Angelopoulos, J. P. McFadden, D. Larson, C. W. Carlson, S. B. Mende, H. Frey, T. Phan, D. G. Sibeck, K.-H. Glassmeier, U. Auster, E. Donovan, I. R. Mann, I. J. Rae, C. T. Russell, A. Runov, X.-Z. Zhou, and L. Kepko. Tail Reconnection Triggering Substorm Onset. *Science*, 321:931–935, August 2008. doi: 10.1126/science.1160495.
- [3] Vassilis Angelopoulos, Anton Artemyev, Tai D. Phan, and Yukinaga Miyashita. Near-Earth magnetotail reconnection powers space storms. *Nature Physics*, 16(3):317–321, January 2020. doi: 10.1038/s41567-019-0749-4.

- [4] V. A. Sergeev, R. J. Pellinen, and T. I. Pulkkinen. Steady Magnetospheric Convection: A Review of Recent Results. *Space Sci. Rev.*, 75:551–604, February 1996. doi: 10.1007/BF00833344.
- [5] S. E. Milan, M. T. Walach, J. A. Carter, H. Sangha, and B. J. Anderson. Substorm Onset Latitude and the Steadiness of Magnetospheric Convection. *Journal of Geophysical Research (Space Physics)*, 124(3):1738–1752, March 2019. doi: 10.1029/2018JA025969.
- [6] A. Runov, V. A. Sergeev, R. Nakamura, W. Baumjohann, S. Apatenkov, Y. Asano, T. Takada, M. Volwerk, Z. Vörös, T. L. Zhang, J.-A. Sauvaud, H. Rème, and A. Balogh. Local structure of the magnetotail current sheet: 2001 Cluster observations. *Annales Geophysicae*, 24:247–262, March 2006.
- [7] A. Runov, V. Angelopoulos, V. A. Sergeev, K.-H. Glassmeier, U. Auster, J. McFadden, D. Larson, and I. Mann. Global properties of magnetotail current sheet flapping: THEMIS perspectives. *Annales Geophysicae*, 27:319–328, January 2009.
- [8] V. A. Sergeev, D. A. Sormakov, S. V. Apatenkov, W. Baumjohann, R. Nakamura, A. V. Runov, T. Mukai, and T. Nagai. Survey of large-amplitude flapping motions in the midtail current sheet. *Annales Geophysicae*, 24:2015–2024, August 2006.
- [9] A. A. Petrukovich, A. V. Artemyev, I. Y. Vasko, R. Nakamura, and L. M. Zelenyi. Current sheets in the Earth magnetotail: plasma and magnetic field structure with Cluster project observations. *Space Sci. Rev.*, 188:311–337, 2015. doi: 10.1007/s11214-014-0126-7.
- [10] Anton Artemyev, San Lu, Mostafa El-Alaoui, Yu Lin, Vassilis Angelopoulos, Xiao-Jia Zhang, Andrei Runov, Ivan Vasko, Lev Zelenyi, and Christopher Russell. Configuration of the Earth’s Magnetotail Current Sheet. *Geophys. Res. Lett.*, 48(6):e92153, March 2021. doi: 10.1029/2020GL092153.
- [11] N. A. Tsyganenko. Data-based modelling of the Earth’s dynamic magnetosphere: a review. *Annales Geophysicae*, 31:1745–1772, October 2013. doi: 10.5194/angeo-31-1745-2013.
- [12] N. A. Tsyganenko. Modeling the Earth’s magnetospheric magnetic field confined within a realistic magnetopause. *J. Geophys. Res.*, 100:5599–5612, April 1995. doi: 10.1029/94JA03193.
- [13] N. A. Tsyganenko. A model of the near magnetosphere with a dawn-dusk asymmetry 1. Mathematical structure. *J. Geophys. Res.*, 107:1179, August 2002. doi: 10.1029/2001JA000219.
- [14] N. A. Tsyganenko and M. I. Sitnov. Modeling the dynamics of the inner magnetosphere during strong geomagnetic storms. *J. Geophys. Res.*, 110:A03208, March 2005. doi: 10.1029/2004JA010798.
- [15] M. I. Sitnov, G. K. Stephens, N. A. Tsyganenko, Y. Miyashita, V. G. Merkin, T. Motoba, S. Ohtani, and K. J. Genestreti. Signatures of Nonideal Plasma Evolution During Substorms Obtained by Mining Multimission Magnetometer Data. *Journal of Geophysical Research (Space Physics)*, 124(11):8427–8456, Nov 2019. doi: 10.1029/2019JA027037.
- [16] G. K. Stephens, M. I. Sitnov, A. Y. Ukhorskiy, E. C. Roelof, N. A. Tsyganenko, and G. Le. Empirical modeling of the storm time innermost magnetosphere using Van Allen Probes and THEMIS data: Eastward and banana currents. *J. Geophys. Res.*, 121:157–170, January 2016. doi: 10.1002/2015JA021700.

- [17] G. K. Stephens, M. I. Sitnov, H. Korth, N. A. Tsyganenko, S. Ohtani, M. Gkioulidou, and A. Y. Ukhorskiy. Global Empirical Picture of Magnetospheric Substorms Inferred From Multimission Magnetometer Data. *Journal of Geophysical Research (Space Physics)*, 124(2):1085–1110, Feb 2019. doi: 10.1029/2018JA025843.
- [18] M. I. Sitnov, G. K. Stephens, T. Motoba, and M. Swisdak. Data Mining Reconstruction of Magnetotail Reconnection and Implications for Its First-Principle Modeling. *Front. Phys.*, 2021. doi: 10.3389/fphy.2021.644884.
- [19] V. Sergeev, V. Angelopoulos, M. Kubyshkina, E. Donovan, X.-Z. Zhou, A. Runov, H. Singer, J. McFadden, and R. Nakamura. Substorm growth and expansion onset as observed with ideal ground-spacecraft THEMIS coverage. *J. Geophys. Res.*, 116:A00I26, February 2011. doi: 10.1029/2010JA015689.
- [20] V. Sergeev, Y. Nishimura, M. Kubyshkina, V. Angelopoulos, R. Nakamura, and H. Singer. Magnetospheric location of the equatorward prebreakup arc. *Journal of Geophysical Research (Space Physics)*, 117(A1):A01212, January 2012. doi: 10.1029/2011JA017154.
- [21] S. Dubyagin, N. Ganushkina, S. Apatenkov, M. Kubyshkina, H. Singer, and M. Liemohn. Geometry of duskside equatorial current during magnetic storm main phase as deduced from magnetospheric and low-altitude observations. *Annales Geophysicae*, 31:395–408, 2013. doi: 10.5194/angeo-31-395-2013.
- [22] W. L. Imhof, J. B. Reagan, and E. E. Gaines. Studies of the sharply defined L dependent energy threshold for isotropy at the midnight trapping boundary. *J. Geophys. Res.*, 84:6371–6384, November 1979. doi: 10.1029/JA084iA11p06371.
- [23] V. A. Sergeev and N. A. Tsyganenko. Energetic particle losses and trapping boundaries as deduced from calculations with a realistic magnetic field model. *Plan. Sp. Sci.*, 30:999–1006, October 1982. doi: 10.1016/0032-0633(82)90149-0.
- [24] V. A. Sergeev, E. M. Sazhina, N. A. Tsyganenko, J. A. Lundblad, and F. Soraas. Pitch-angle scattering of energetic protons in the magnetotail current sheet as the dominant source of their isotropic precipitation into the nightside ionosphere. *Plan. Sp. Sci.*, 31:1147–1155, October 1983. doi: 10.1016/0032-0633(83)90103-4.
- [25] J. Büchner and L. M. Zelenyi. Regular and chaotic charged particle motion in magnetotaillike field reversals. I - Basic theory of trapped motion. *J. Geophys. Res.*, 94:11821–11842, September 1989. doi: 10.1029/JA094iA09p11821.
- [26] D. C. Delcourt, J. A. Sauvaud, R. F. Martin, and T. E. Moore. Gyrophase effects in the centrifugal impulse model of particle motion in the magnetotail. *J. Geophys. Res.*, 100:17211–17220, September 1995. doi: 10.1029/95JA00657.
- [27] A. V. Artemyev, V. Angelopoulos, and A. Runov. On the radial force balance in the quiet time magnetotail current sheet. *J. Geophys. Res.*, 121:4017–4026, May 2016. doi: 10.1002/2016JA022480.
- [28] L. D. Landau and E. M. Lifshitz. *Vol. 1: Mechanics*. Course of Theoretical Physics. Oxford: Pergamon Press, 1st edition, 1960.
- [29] A. A. Slutskin. Motion of a one-dimensional nonlinear oscillator under adiabatic conditions. *Soviet JETP*, 18:676–682, 1964.

- [30] A. I. Neishtadt. On the accuracy of persistence of adiabatic invariant in single-frequency system. *Regular and chaotic dynamics*, 5:213–218, 2000. doi: 10.1070/RD2000v005n02ABEH000143.
- [31] B. V. Chirikov. Stability of the motion of a charged particle in a magnetic confinement system. *Soviet Journal of Plasma Physics*, 4:521–541, June 1978.
- [32] B. V. Chirikov. A universal instability of many-dimensional oscillator systems. *Physics Reports*, 52:263–379, May 1979. doi: 10.1016/0370-1573(79)90023-1.
- [33] J. E. Howard. Nonadiabatic Particle Motion in Cusped Magnetic Fields. *Physics of Fluids*, 14: 2378–2384, November 1971. doi: 10.1063/1.1693344.
- [34] R. H. Cohen, G. Rowlands, and J. H. Foote. Nonadiabaticity in mirror machines. *Physics of Fluids*, 21:627–644, April 1978. doi: 10.1063/1.862271.
- [35] T. J. Birmingham. Pitch angle diffusion in the Jovian magnetodisc. *J. Geophys. Res.*, 89: 2699–2707, May 1984. doi: 10.1029/JA089iA05p02699.
- [36] D. C. Delcourt, R. F. Martin, Jr., and F. Alem. A simple model of magnetic moment scattering in a field reversal. *Geophys. Res. Lett.*, 21:1543–1546, July 1994. doi: 10.1029/94GL01291.
- [37] D. C. Delcourt, J.-A. Sauvaud, R. F. Martin, and T. E. Moore. On the nonadiabatic precipitation of ions from the near-Earth plasma sheet. *J. Geophys. Res.*, 101:17409–17418, August 1996. doi: 10.1029/96JA01006.
- [38] S. L. Young, R. E. Denton, B. J. Anderson, and M. K. Hudson. Empirical model for μ scattering caused by field line curvature in a realistic magnetosphere. *J. Geophys. Res.*, 107:1069, June 2002. doi: 10.1029/2000JA000294.
- [39] S. L. Young, R. E. Denton, B. J. Anderson, and M. K. Hudson. Magnetic field line curvature induced pitch angle diffusion in the inner magnetosphere. *J. Geophys. Res.*, 113:3210, March 2008. doi: 10.1029/2006JA012133.
- [40] A. G. Yahnin, V. A. Sergeev, B. B. Gvozdevsky, and S. Vennerstrøm. Magnetospheric source region of discrete auroras inferred from their relationship with isotropy boundaries of energetic particles. *Annales Geophysicae*, 15:943–958, August 1997. doi: 10.1007/s00585-997-0943-z.
- [41] V. A. Sergeev, I. A. Chernyaev, V. Angelopoulos, and N. Y. Ganushkina. Magnetospheric conditions near the equatorial footpoints of proton isotropy boundaries. *Annales Geophysicae*, 33:1485–1493, December 2015. doi: 10.5194/angeo-33-1485-2015.
- [42] S. Dubyagin, N. Yu. Ganushkina, and V. Sergeev. Formation of 30 KeV Proton Isotropic Boundaries During Geomagnetic Storms. *Journal of Geophysical Research (Space Physics)*, 123 (5):3436–3459, May 2018. doi: 10.1002/2017JA024587.
- [43] V. A. Sergeev, E. I. Gordeev, V. G. Merkin, and M. I. Sitnov. Does a Local B-Minimum Appear in the Tail Current Sheet During a Substorm Growth Phase? *Geophys. Res. Lett.*, 45: 2566–2573, March 2018. doi: 10.1002/2018GL077183.
- [44] S. Dubyagin, S. Apatenkov, E. Gordeev, N. Ganushkina, and Y. Zheng. Conditions of Loss Cone Filling by Scattering on the Curved Field Lines for 30 keV Protons During Geomagnetic Storm as Inferred From Numerical Trajectory Tracing. *Journal of Geophysical Research (Space Physics)*, 126(1):e28490, January 2021. doi: 10.1029/2020JA028490.

- [45] D. C. Delcourt, H. V. Malova, and L. M. Zelenyi. Quasi-adiabaticity in bifurcated current sheets. *Geophys. Res. Lett.*, 33:6106, March 2006. doi: 10.1029/2005GL025463.
- [46] D. C. Delcourt, D. A. Ovodkov, V. Y. Popov, H. V. Malova, and L. M. Zelenyi. Do phase portraits resist current sheet bifurcation? *Advances in Space Research*, 37:547–551, 2006. doi: 10.1016/j.asr.2005.02.071.
- [47] M. I. Sitnov, M. Swisdak, and A. V. Divin. Dipolarization fronts as a signature of transient reconnection in the magnetotail. *J. Geophys. Res.*, 114:A04202, April 2009. doi: 10.1029/2008JA013980.
- [48] A. Runov, V. Angelopoulos, M. I. Sitnov, V. A. Sergeev, J. Bonnell, J. P. McFadden, D. Larson, K.-H. Glassmeier, and U. Auster. THEMIS observations of an earthward-propagating dipolarization front. *Geophys. Res. Lett.*, 36:L14106, July 2009. doi: 10.1029/2009GL038980.
- [49] V. Angelopoulos, A. Runov, X. Z. Zhou, D. L. Turner, S. A. Kiehas, S. S. Li, and I. Shinohara. Electromagnetic Energy Conversion at Reconnection Fronts. *Science*, 341:1478–1482, 2013. doi: 10.1126/science.1236992.
- [50] H. S. Fu, J. B. Cao, Y. V. Khotyaintsev, M. I. Sitnov, A. Runov, S. Y. Fu, M. Hamrin, M. André, A. Retinò, Y. D. Ma, H. Y. Lu, X. H. Wei, and S. Y. Huang. Dipolarization fronts as a consequence of transient reconnection: In situ evidence. *Geophys. Res. Lett.*, 40:6023–6027, December 2013. doi: 10.1002/2013GL058620.
- [51] S. Dubyagin, V. Sergeev, S. Apatenkov, V. Angelopoulos, A. Runov, R. Nakamura, W. Baumjohann, J. McFadden, and D. Larson. Can flow bursts penetrate into the inner magnetosphere? *Geophys. Res. Lett.*, 38:L08102, April 2011. doi: 10.1029/2011GL047016.
- [52] J. Liu, V. Angelopoulos, X.-Z. Zhou, and A. Runov. Magnetic flux transport by dipolarizing flux bundles. *J. Geophys. Res.*, 119:909–926, February 2014. doi: 10.1002/2013JA019395.
- [53] E. Yushkov, A. Petrukovich, A. Artemyev, and R. Nakamura. Thermodynamics of the magnetotail current sheet thinning. *Journal of Geophysical Research: Space Physics*, 126(4):e2020JA028969, 2021. doi: <https://doi.org/10.1029/2020JA028969>.
- [54] A. Runov, V. Angelopoulos, M. Sitnov, V. A. Sergeev, R. Nakamura, Y. Nishimura, H. U. Frey, J. P. McFadden, D. Larson, J. Bonnell, K.-H. Glassmeier, U. Auster, M. Connors, C. T. Russell, and H. J. Singer. Dipolarization fronts in the magnetotail plasma sheet. *Plan. Sp. Sci.*, 59:517–525, May 2011. doi: 10.1016/j.pss.2010.06.006.
- [55] K.-J. Hwang, M. L. Goldstein, E. Lee, and J. S. Pickett. Cluster observations of multiple dipolarization fronts. *J. Geophys. Res.*, 116:A00I32, April 2011. doi: 10.1029/2010JA015742.
- [56] Y. V. Khotyaintsev, C. M. Cully, A. Vaivads, M. André, and C. J. Owen. Plasma Jet Braking: Energy Dissipation and Nonadiabatic Electrons. *Physical Review Letters*, 106(16):165001, April 2011. doi: 10.1103/PhysRevLett.106.165001.
- [57] H. S. Fu, Y. V. Khotyaintsev, A. Vaivads, M. André, and S. Y. Huang. Electric structure of dipolarization front at sub-proton scale. *Geophys. Res. Lett.*, 39:L06105, March 2012. doi: 10.1029/2012GL051274.

- [58] A. Runov, V. Angelopoulos, X.-Z. Zhou, X.-J. Zhang, S. Li, F. Plaschke, and J. Bonnell. A THEMIS multicase study of dipolarization fronts in the magnetotail plasma sheet. *J. Geophys. Res.*, 116:A05216, May 2011. doi: 10.1029/2010JA016316.
- [59] A. Runov, V. Angelopoulos, C. Gabrielse, J. Liu, D. L. Turner, and X.-Z. Zhou. Average thermodynamic and spectral properties of plasma in and around dipolarizing flux bundles. *J. Geophys. Res.*, 120:4369–4383, June 2015. doi: 10.1002/2015JA021166.
- [60] L. M. Zelenyi, A. I. Neishtadt, A. V. Artemyev, D. L. Vainchtein, and H. V. Malova. Quasia-adiabatic dynamics of charged particles in a space plasma. *Physics Uspekhi*, 56:347, April 2013. doi: 10.3367/UFNe.0183.201304b.0365.
- [61] B. J. Anderson, R. B. Decker, N. P. Paschalidis, and T. Sarris. Onset of nonadiabatic particle motion in the near-Earth magnetotail. *J. Geophys. Res.*, 102:17553–17570, August 1997. doi: 10.1029/97JA00798.
- [62] W. W. Eshetu, J. G. Lyon, M. K. Hudson, and M. J. Wiltberger. Pitch Angle Scattering of Energetic Electrons by BBFs. *Journal of Geophysical Research (Space Physics)*, 123(11): 9265–9274, November 2018. doi: 10.1029/2018JA025788.
- [63] V. I. Arnold, V. V. Kozlov, and A. I. Neishtadt. *Mathematical Aspects of Classical and Celestial Mechanics*. Dynamical Systems III. Encyclopedia of Mathematical Sciences. Springer-Verlag, New York, 3rd edition, 2006.
- [64] P. I. Shustov, A. V. Artemyev, and E. V. Yushkov. Intermediate regime of charged particle scattering in the field-reversal configuration. *Chaos*, 25(12):123118, December 2015. doi: 10.1063/1.4938535.
- [65] A. Runov, V. Angelopoulos, and X.-Z. Zhou. Multipoint observations of dipolarization front formation by magnetotail reconnection. *J. Geophys. Res.*, 117:A05230, May 2012. doi: 10.1029/2011JA017361.
- [66] F. Hertweck and A. Schlüter. Die „adiabatische Invarianz“ des magnetischen Bahnmoments geladener Teilchen. *Zeitschrift Naturforschung Teil A*, 12:844, October 1957.
- [67] A. M. Dykhne. Quantum transitions in the adiabatic approximation. *Soviet JETP*, 11:411–415, 1960.
- [68] P. O. Vandervoort. The nonconstancy of the adiabatic invariants. *Annals of Physics*, 12: 436–443, March 1961. doi: 10.1016/0003-4916(61)90070-7.
- [69] T. Su. On the accuracy of conservation of adiabatic invariants in slow-fast Hamiltonian systems. *Regular and Chaotic Dynamics*, 17:54–62, February 2012. doi: 10.1134/S1560354712010054.
- [70] A. M. Dykhne and A. V. Chaplik. Variation of the adiabatic invariant for a particle in a magnetic field. II. *Soviet JETP*, 13:465–467, 1961.
- [71] A. Neishtadt. The separation of motions in systems with rapidly rotating phase. *Journal of Applied Mathematics and Mechanics*, 48:133–139, 1984. doi: 10.1016/0021-8928(84)90078-9.
- [72] A. Vasiliev, A. Neishtadt, A. Artemyev, and L. Zelenyi. Jump of the adiabatic invariant at a separatrix crossing: Degenerate cases. *Physica D Nonlinear Phenomena*, 241:566–573, March 2012. doi: 10.1016/j.physd.2011.11.015.

- [73] D. C. Delcourt, G. Belmont, J.-A. Sauvaud, T. E. Moore, and R. F. Martin. Centrifugally driven phase bunching and related current sheet structure in the near-Earth magnetotail. *J. Geophys. Res.*, 101:19839, September 1996. doi: 10.1029/96JA01772.
- [74] V. Angelopoulos, E. Tsai, L. Bingley, C. Shaffer, D. L. Turner, A. Runov, W. Li, J. Liu, A. V. Artemyev, X. J. Zhang, R. J. Strangeway, R. E. Wirz, Y. Y. Shprits, V. A. Sergeev, R. P. Caron, M. Chung, P. Cruce, W. Greer, E. Grimes, K. Hector, M. J. Lawson, D. Leneman, E. V. Masongsong, C. L. Russell, C. Wilkins, D. Hinkley, J. B. Blake, N. Adair, M. Allen, M. Anderson, M. Arreola-Zamora, J. Artinger, J. Asher, D. Branchevsky, M. R. Capitelli, R. Castro, G. Chao, N. Chung, M. Cliffe, K. Colton, C. Costello, D. Depe, B. W. Domae, S. Eldin, L. Fitzgibbon, A. Flemming, I. Fox, D. M. Frederick, A. Gilbert, A. Gildemeister, A. Gonzalez, B. Hesford, S. Jha, N. Kang, J. King, R. Krieger, K. Lian, J. Mao, E. McKinney, J. P. Miller, A. Norris, M. Nuesca, A. Palla, E. S. Y. Park, C. E. Pedersen, Z. Qu, R. Rozario, E. Rye, R. Seaton, A. Subramanian, S. R. Sundin, A. Tan, W. Turner, A. J. Villegas, M. Wasden, G. Wing, C. Wong, E. Xie, S. Yamamoto, R. Yap, A. Zarifian, and G. Y. Zhang. The ELFEN Mission. *Space Sci. Rev.*, 216(5):103, July 2020. doi: 10.1007/s11214-020-00721-7.
- [75] A. T. Johnson, M. Shumko, B. Griffith, D. M. Klumpar, J. Sample, L. Springer, N. Leh, H. E. Spence, S. Smith, A. Crew, M. Handley, K. M. Mashburn, B. A. Larsen, and J. B. Blake. The FIREBIRD-II CubeSat mission: Focused investigations of relativistic electron burst intensity, range, and dynamics. *Review of Scientific Instruments*, 91(3):034503, March 2020. doi: 10.1063/1.5137905.